Supplementary materials

Dynamics study of the post-transition-state-bifurcation process of the $(HCOOH)H^+ \rightarrow CO + H_3O^+ / HCO^+ + H_2O$ dissociation: Application of machine-learning techniques

Tatsuhiro Murakami [*,†,1,2], Shunichi Ibuki[1], Yu Hashimoto[1], Yuya Kikuma[1], and Toshiyuki Takayanagi [‡,1]

[1]Department of Chemistry, Saitama University, Shimo-Okubo 255, Sakura-ku, Saitama City, Saitama, 338-8570, Japan
[2]Department of Materials & Life Sciences, Faculty of Science & Technology, Sophia University, 7-1 Kioicho, Chiyoda-ku, Tokyo, 102-8554, Japan

Contents

*Corresponding author
†E-mail: murakamit@mail.saitama-u.ac.jp, ORCID: 0000-0001-8904-8673
‡E-mail: tako@mail.saitama-u.ac.jp, ORCID:0000-0003-0563-9236

S1 Figures and Tables for the supporting information

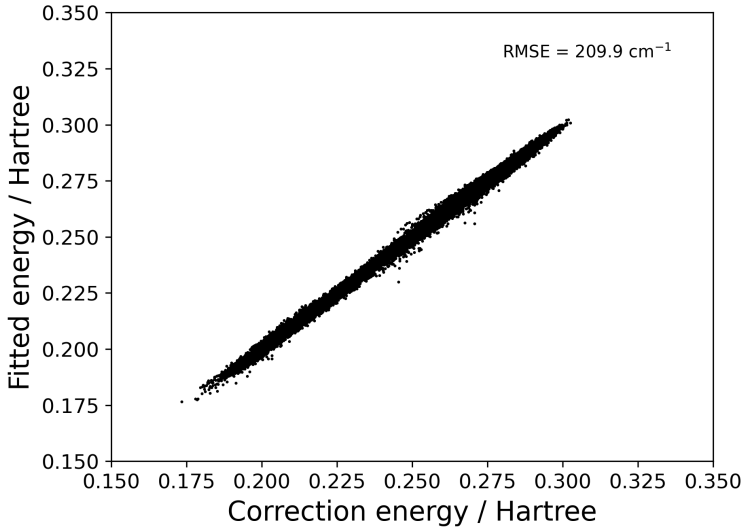

Figure S1: The fitted potential energy as a function of the correction energy

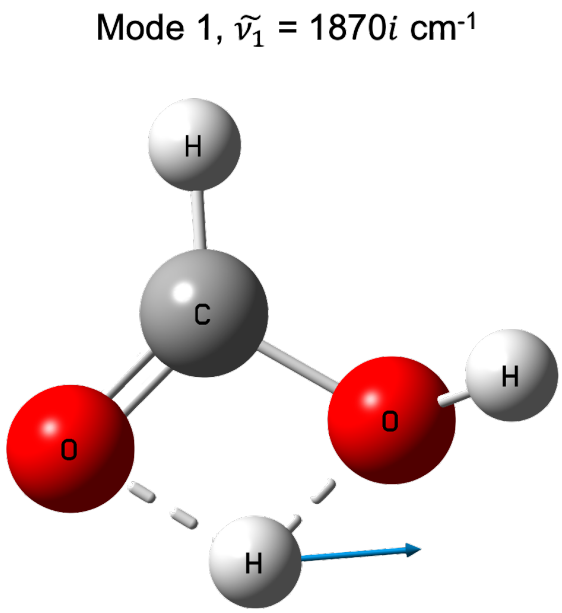

Figure S2: Normal mode vector with the vibrational frequency $\tilde{\nu}_1$ for the imaginary frequency mode 1 at the transition state TS_{1-2}

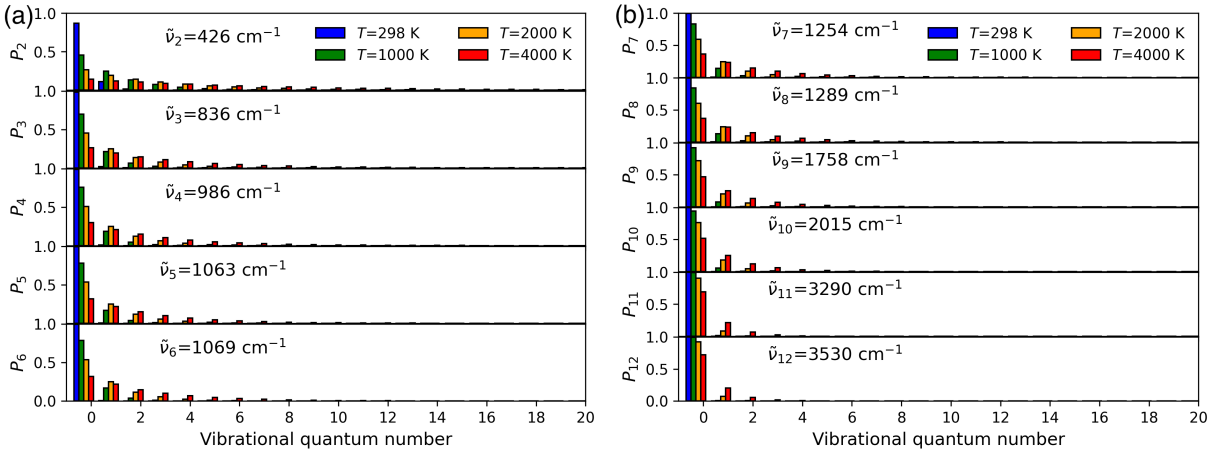

Figure S3: Temperature-dependent populations of vibrational states with normal mode frequencies. The blue, green, orange and red bars represent the populations at 298, 1000, 2000 and 4000 K for (a) modes 2-6 and (b) modes 7-12.

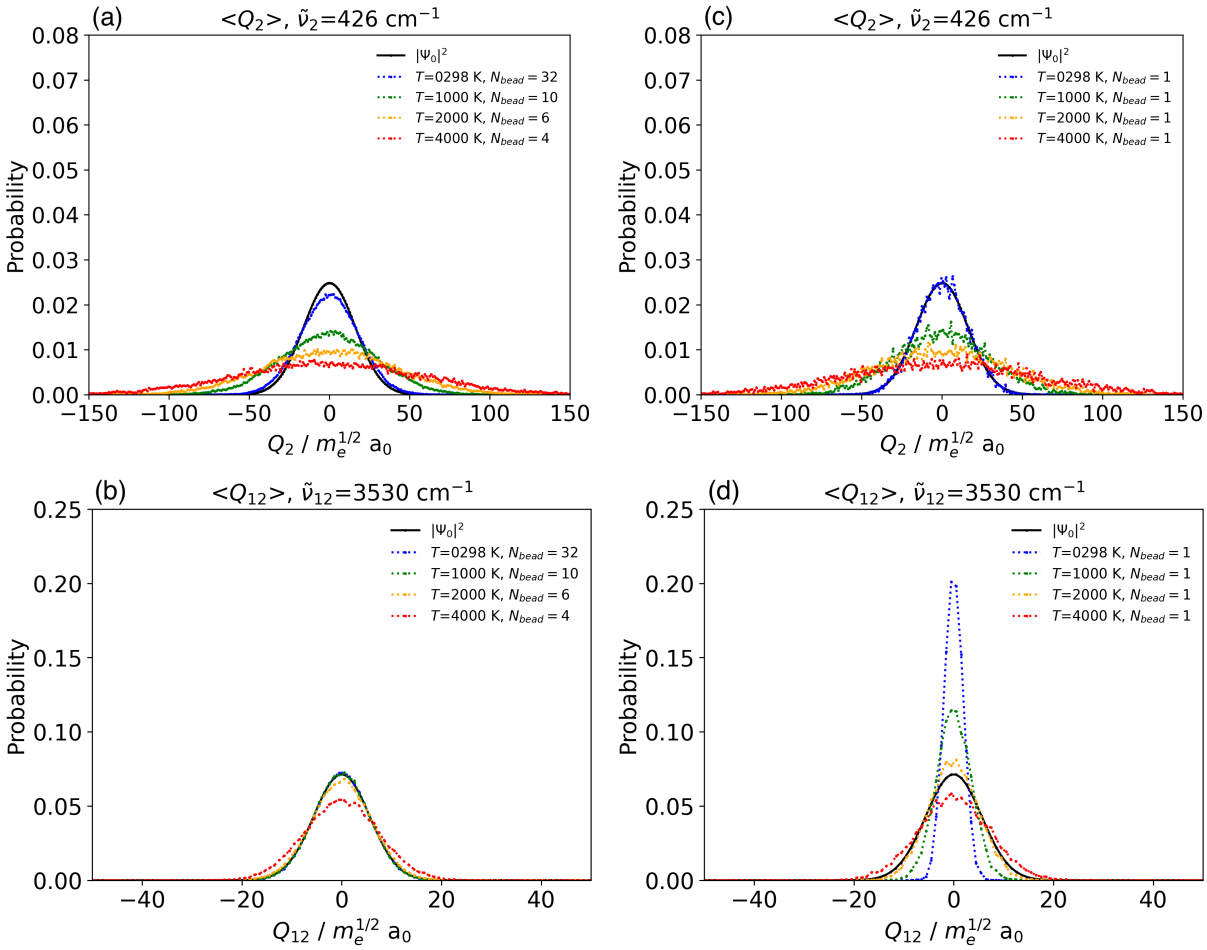

Figure S4: The distribution of the expectation values of the configuration spaces (a) for Q_2 and (b) Q_{12} modes by PIMD sampling, and (c) for Q_2 and (d) Q_{12} modes by classical sampling. The blue, green, orange and red dotted lines represent the coordinate expectation values for 298, 1000, 2000 and 4000 K. The black sold line present the magnitude of the zero-point vibrational wave function $|\Psi_0|^2$

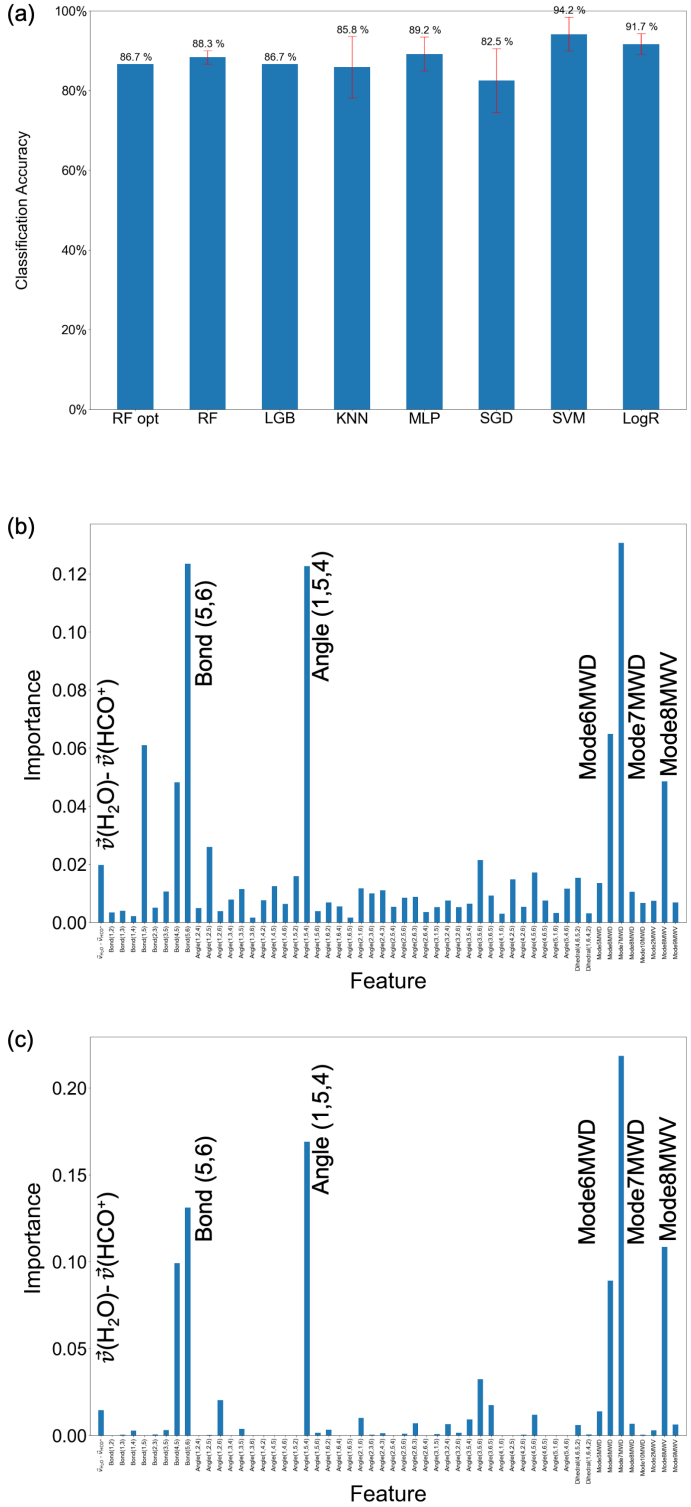

Figure S5: (a) Accuracy scores and importance of the 54 features for (b) RF and (c) LGB models using 120 data in the binary classification in terms of the classical MD simulations at 298 K

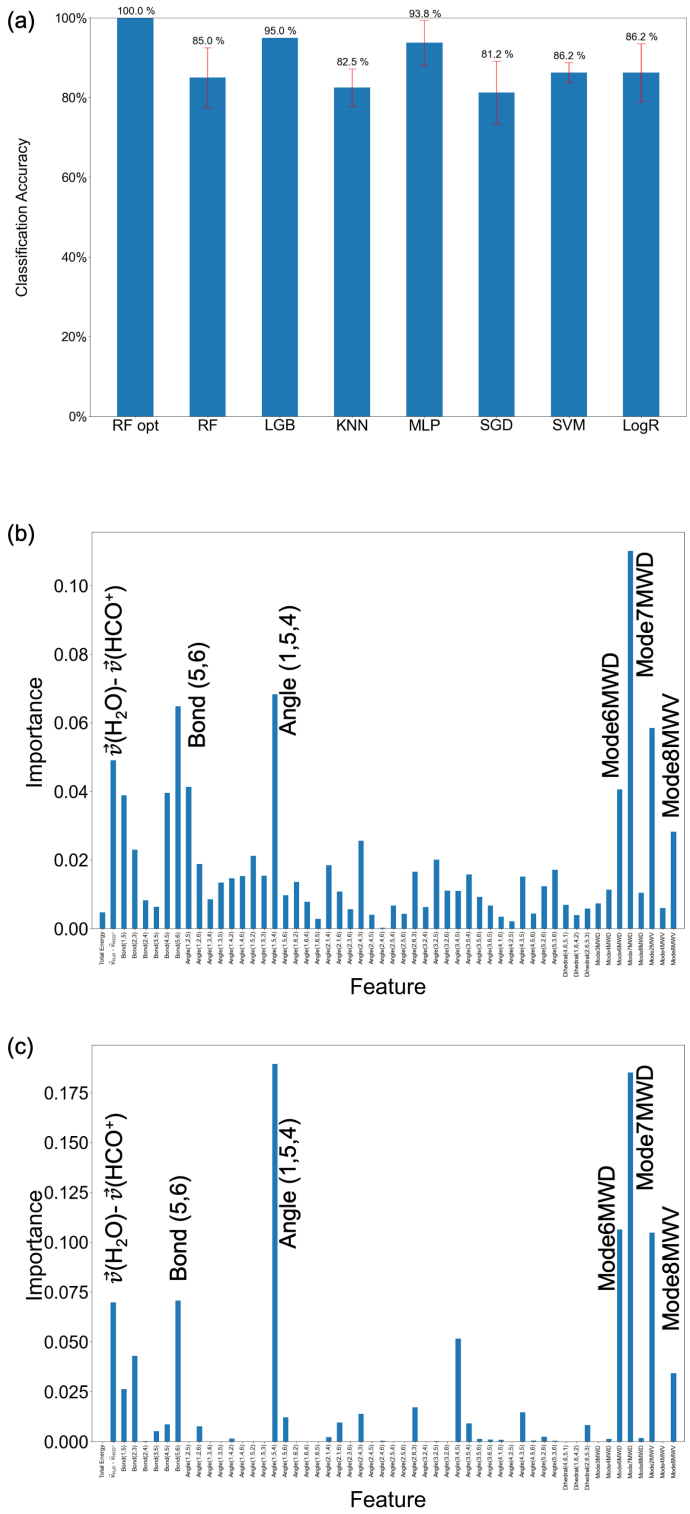

Figure S6: (a) Accuracy scores and importance of the 54 features for (b) RF and (c) LGB models using 80 data in the binary classification in terms of the classical MD simulations at 298 K

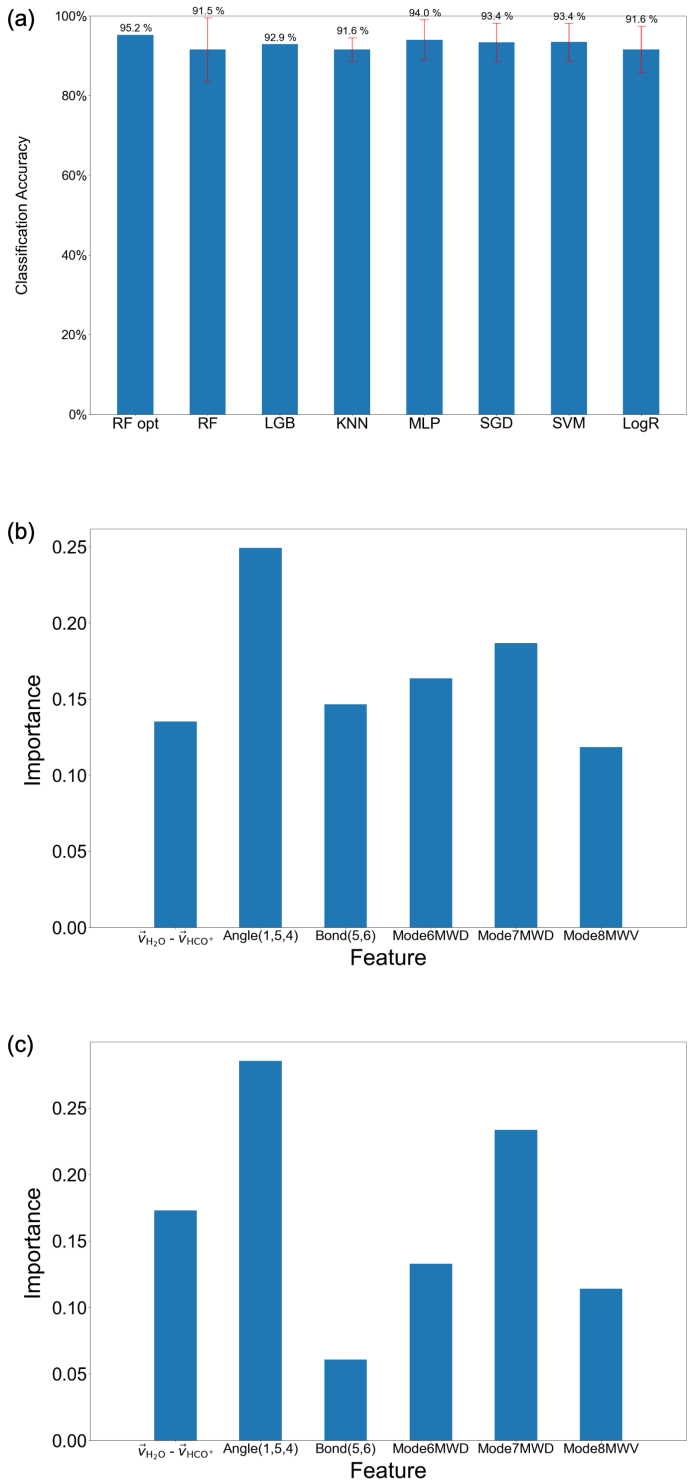

Figure S7: (a) Accuracy scores and importance of the six features for (b) RF and (c) LGB models using 166 data in the binary classification in terms of the classical MD simulations at 298 K

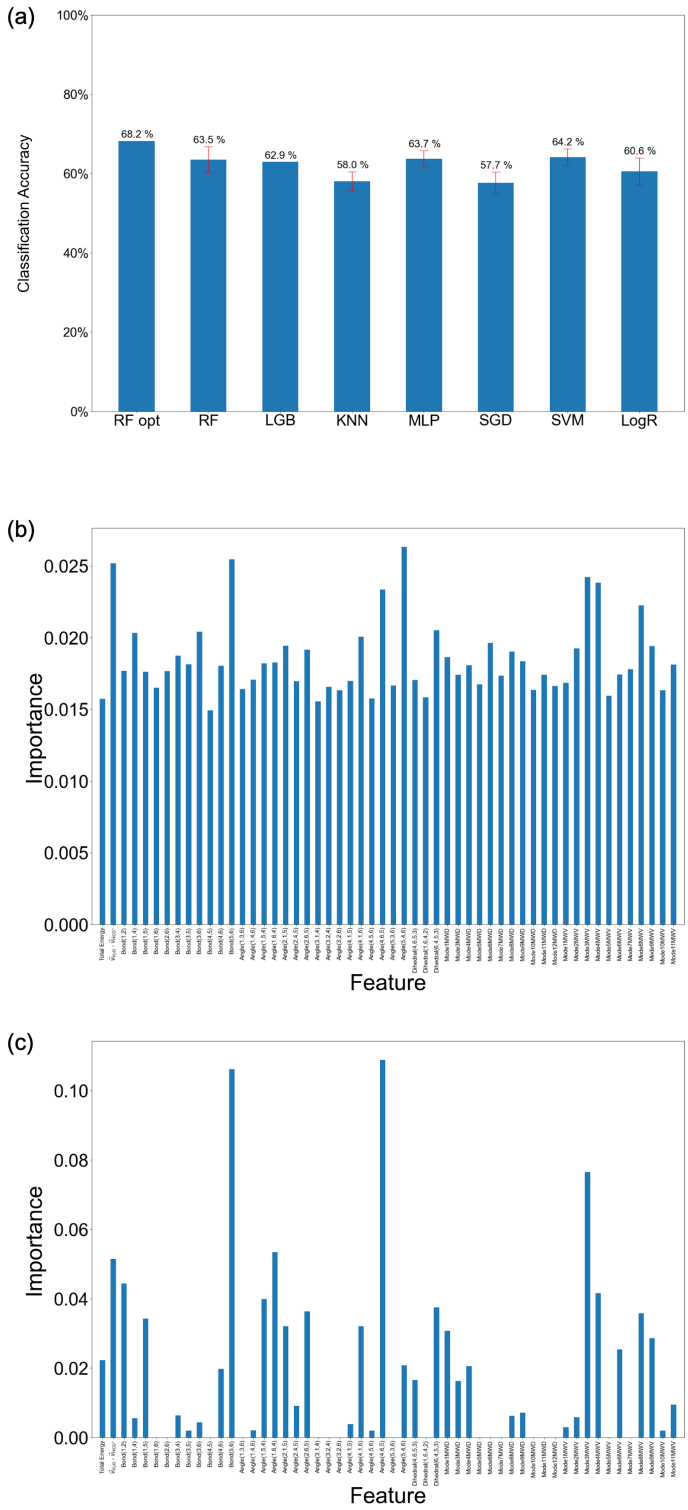

Figure S8: (a) Accuracy scores and importance of 54 transition-state features for (b) RF and (c) LGB models in the binary classification with respect to the 4000 K classical simulation

Table S1: The potential energies at key geometries calculated by our PES (in kcal mol^{-1}) and MP2/6-31G(d), and the comparison with the previous study (MP2/6-31G(d))

Coordinate	PES	MP2	Ref. [1]
EQ_1	0.0	0.0	0.0
TS_{1-2}	49.0	52.2	47.8
INT_2	14.1	17.7	15.1
TS_{2-3}	19.8	20.7	16.5
INT_3	0.9	3.7	0.7
TS_{3-4}	17.4	18.4	-
INT_4	8.5	11.5	-
$HCO^+ + H_2O$	40.8	46.5	39.7
$CO + H_3O^+$	19.2	20.9	16.3

Table S2: The zero-point vibrational energies (ZPE), the expectation values of internal energy by PIMD simulations $< E >$ and the analytical values $< U_q >$ (in kcal mol^{-1}) for each temperature with different frequencies $\tilde{\nu}_\alpha$

		298 K		1000 K	
$\tilde{\nu}_\alpha$	ZPE	$< E >$	$< U_q >$	$< E >$	$< U_q >$
$\tilde{\nu}_2$	0.61	0.78	0.79	2.04	2.05
$\tilde{\nu}_3$	1.20	1.24	1.24	2.22	2.22
$\tilde{\nu}_4$	1.41	1.43	1.43	2.31	2.31
$\tilde{\nu}_5$	1.52	1.54	1.54	2.35	2.36
$\tilde{\nu}_6$	1.53	1.54	1.55	2.35	2.36
$\tilde{\nu}_7$	1.79	1.80	1.80	2.49	2.50
$\tilde{\nu}_8$	1.84	1.84	1.85	2.51	2.53
$\tilde{\nu}_9$	2.51	2.49	2.51	2.92	2.95
$\tilde{\nu}_{10}$	2.88	2.84	2.88	3.18	3.22
$\tilde{\nu}_{11}$	4.70	4.57	4.70	4.68	4.79
$\tilde{\nu}_{12}$	5.05	4.88	5.05	4.97	5.11
		2000 K		4000 K	
$\tilde{\nu}_\alpha$		$< E >$	$< U_q >$	$< E >$	$< U_q >$
$\tilde{\nu}_2$		3.99	4.00	7.95	7.96
$\tilde{\nu}_3$		4.09	4.09	8.00	8.01
$\tilde{\nu}_4$		4.13	4.14	8.02	8.03
$\tilde{\nu}_5$		4.16	4.17	8.04	8.04
$\tilde{\nu}_6$		4.16	4.17	8.03	8.04
$\tilde{\nu}_7$		4.23	4.24	8.08	8.08
$\tilde{\nu}_8$		4.25	4.25	8.09	8.09
$\tilde{\nu}_9$		4.48	4.49	8.18	8.21
$\tilde{\nu}_{10}$		4.63	4.65	8.28	8.29
$\tilde{\nu}_{11}$		5.60	5.68	8.80	8.85
$\tilde{\nu}_{12}$		5.81	5.91	8.93	8.99

Table S3: Temperature-dependent internal energy of the classical Hamiltonian for harmonic oscillator $< U_c >$ and the energy expectation values by classical sampling $< E >$ (in kcal mol^{-1})

	298 K $< U_q >$	1000 K $< U_q >$	2000 K $< U_q >$	4000 K $< U_q >$
	0.59	1.99	3.97	7.95
$\tilde{\nu}_\alpha$	$< E >$	$< E >$	$< E >$	$< E >$
		Classical		
$\tilde{\nu}_2$	0.59	1.99	3.99	7.94
$\tilde{\nu}_3$	0.59	1.98	3.97	7.94
$\tilde{\nu}_4$	0.59	1.98	3.97	7.98
$\tilde{\nu}_5$	0.59	1.99	3.98	7.93
$\tilde{\nu}_6$	0.59	1.99	3.96	7.95
$\tilde{\nu}_7$	0.59	1.99	3.98	7.93
$\tilde{\nu}_8$	0.59	1.99	3.97	7.91
$\tilde{\nu}_9$	0.59	1.99	3.98	7.95
$\tilde{\nu}_{10}$	0.59	1.99	3.98	7.95
$\tilde{\nu}_{11}$	0.59	1.99	3.98	7.96
$\tilde{\nu}_{12}$	0.59	1.99	3.98	7.96

References

[1] Osamu Sekiguchi, Vebjørn Bakken, and Einar Uggerud. Decomposition of protonated formic acid: One transition state - Two product channels. J. Am. Soc. Mass Spectrom., 15(7):982–988, 2004.